Interface engineering for improved light transmittance through photonic crystal flat lenses

G. Scherrer, M. Hofman, W. Smigaj, B. Gralak, X. Melique, O. Vanbesien, D. Lippens, C. Dumas, B. Cluzel, F. de Fornel

Applied Physics Letters

Interface engineering for improved light transmittance through photonic crystal flat lenses

Cite as: Appl. Phys. Lett. **97**, 071119 (2010); https://doi.org/10.1063/1.3473760
Submitted: 28 May 2010 • Accepted: 10 July 2010 • Published Online: 20 August 2010

Geoffroy Scherrer, Maxence Hofman, Wojciech Śmigaj, et al.

Interface engineering for improved light transmittance through photonic crystal flat lenses

Geoffroy Scherrer,[1,a)] Maxence Hofman,[2] Wojciech Śmigaj,[3] Boris Gralak,[3] Xavier Mélique,[2] Olivier Vanbésien,[2] Didier Lippens,[2] Colette Dumas,[1] Benoit Cluzel,[1,b)] and Frédérique de Fornel[1]

[1]*OCP-LICB, UMR CNRS 5209, 9, Avenue A. Savary, BP 47870, 21078 Dijon, France*
[2]*IEMN, UMR CNRS 8520, Université de Lille, BP 60069, F-59652 Villeneuve d'Ascq Cedex, France*
[3]*Institut Fresnel, CNRS, Aix-Marseille Université, Ecole Centrale Marseille, Campus de St Jérôme, 13397 Marseille Cedex 20, France*

(Received 28 May 2010; accepted 10 July 2010; published online 20 August 2010)

In this paper, we present photonic crystal flat lenses with interfaces engineered to improve the light transmittance thanks to a broad angles impedance matching. The interface engineering consists in the realization of antireflection gratings on the edges of the lenses which are designed to reduce the propagative waves reflectivity over a wide range of incident angles. The fabricated structures were measured in optical near-field and a four times enhancement of the light transmission efficiency is reported. © *2010 American Institute of Physics*. [doi:10.1063/1.3473760]

In 1968, Veselago described unusual properties of negative index media such as negative refraction, reversed Doppler effect, or reversed Cerenkov radiation.[1] More recently, the use of negative refraction has enabled the emergence of innovative concepts for optical imaging including flat lenses or Pendry's perfect lenses.[1–3] If several numerical and experimental demonstrations of these concepts were reported with millimeter patterned metallic materials operating at the microwave wavelengths, their counterparts at optical frequencies[3,4] have to face the limitations of metal damping constants and nanopatterning. To overcome these difficulties at optical frequencies, the purely dielectric route, i.e., the photonic crystal (PC) route, is attracted a growing interest. As a matter of fact, under rigorous optogeometrical considerations, PCs can behave as negative index media with a configurable effective refractive index that can be used for lensing or cloaking applications.[5–7]

Among the different PC geometries proposed in the literature, we study here the two-dimensional (2D) PC which consists in a triangular lattice of air holes etched in a semiconductor slab. As demonstrated experimentally elsewhere by different groups and by different methods in far-field and/or in near-field,[8–10] these structures could present a negative refractive index which is isotropic enough to build flat lenses. Obviously, in this field the transmission of the lens is a key figure merit for future applications. This has been theoretically investigated and it has been shown that interface truncation of the 2D PC structures plays a crucial role in the light transmission process, for evanescent as well as for propagative waves.[11–14] In that way, several designs of 2D PC interfaces have been suggested, summarized in Ref. 15 but only few of them have been experimentally tested. The truncation proposed in Ref. 16 is devoted to evanescent waves enhancement by surface mode excitation whereas in Refs. 17 and 18, a hole shape engineering is performed to decrease propagative waves reflectivity at 2D PC input interface. However, the air hole deformation proposed in Ref. 17 has a restricted angular tolerance and its experimental demonstration effect is made indirectly in far-field. Although direct near-field observations of the effect of a tapered air holes layer are shown in Ref. 18, no focusing regime, only negative refraction, is reported. In this work, we fabricated a 2D PC flat lens with input and output interfaces engineered in order to improve the lens transmittance with a broad angular acceptance and we quantify experimentally the transmission improvement using scanning near-field optical microscopy (SNOM) observations.

The structure considered here is a 2D PC flat lens made of a triangular lattice of air holes etched in a semiconductor heterostructure (1.6 μm InP/0.5 μm InGaAsP /0.2 μm InP). The total height of the heterostructure from the substrate to air is 2.3 μm height. As shown elsewhere,[10] this structure provides an isotropic effective negative index of $n=-1$ which is achieved for a transverse electric polarized mode (TE, electric field parallel to the hole axis) at a reduced frequency of $a/\lambda=0.307$, a being the lattice parameter of the 2D PC and λ the operating wavelength. For $\lambda=1550$ nm, the associated a is 476 nm and the air hole diameter is 350 nm. Furthermore, a monomode ridge waveguide tapered to 400 nm mimics a subwavelength source point. The complete sample (waveguide+lens) is embedded in air. With such a structure, a negative refraction focusing regime of light at optical frequencies has been already demonstrated.[10] However, the mismatch between free space impedance and impedance of propagative waves inside the lens, i.e., the Bloch waves,[19,20] is a severe limitation since the light transmission efficiency of this lens (LTE defined as the ratio between image and source light intensity) was measured to be lower than 1%. Here, we started the improvement of the lens LTE by reducing its total length from 21 rows of air holes to 13 rows. This leads to an increase in the LTE from less than 1% to 5%. As a matter of fact, to preserve the symmetry between the source and the image planes compared to the center of a lens with $n=-1$, the shorter the lens is, the shorter the distance between the lens input and the end of the waveguide. As a consequence, due to out-of-plane diffraction, the coupling efficiency between the light radiated by the waveguide and the Bloch waves inside the lens is increased. We shall

[a)]Electronic mail: geoffroy.scherrer@u-bourgogne.fr.
[b)]Electronic mail: benoit.cluzel@u-bourgogne.fr.

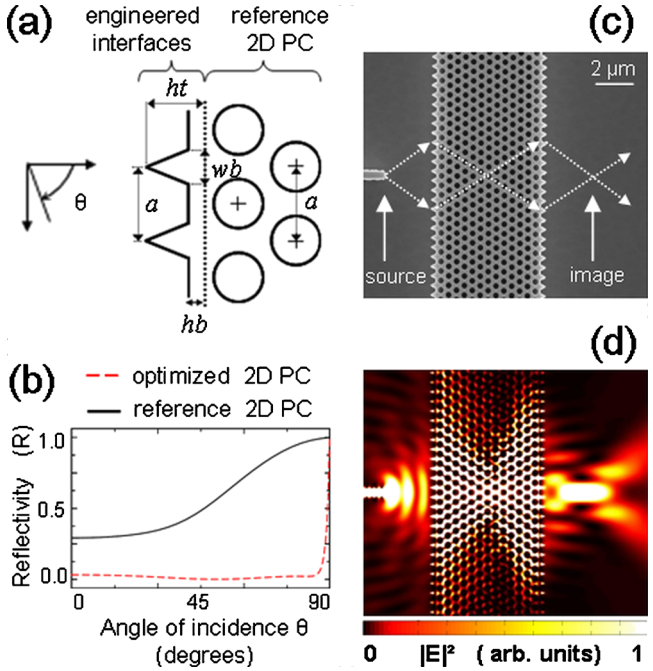

FIG. 1. (Color online) (a) Schematic top view of the 2D PC lens covered with the triangular pattern. (b) Reflectivity of reference and optimized (ideal case for $\lambda=1530$ nm) semi-infinite 2D PCs as functions of the angle of incidence. (c) SEM view of one fabricated optimized lens with the associated waveguide. A ray tracing corresponding to an effective negative index of $n=-1$ is superimposed. (d) 2D FDTD simulations of the electric field intensity plane distribution at 1550 nm for the ideal optimized lens. (c) and (d) are plotted at the same scale.

consider the 13 rows structure as the reference lens (thickness of 5.5 μm).

Next, we engineered the interfaces of this reference lens in the way proposed in Ref. 15. We use a triangular antireflection grating etched on the two interfaces of the lens. As shown in Fig. 1(a), the gratings is defined by the three parameters *wb*, *hb*, and *ht* of the periodic triangular pattern (periodicity is set to the lattice parameter *a*). In the following, the reference lens sandwiched with this periodic triangular pattern will be called the optimized lens. A numerical optimization procedure, similar to that from Ref. 15, yields the ideal triangular pattern defined by $wb=0.50a$, $hb=0.01a$, and $ht=0.69a$ for the shifted operating wavelength $\lambda=1530$ nm. Indeed, our previous works[10] has revealed a spectral shift between 2D simulated lens design (for $\lambda=1550$ nm) and the optimal configuration for SNOM measurements (at $\lambda=1530$ nm). The reflectivity angular dependence of the reference and the optimized (ideal case) semi-infinite 2D PCs are shown in Fig. 1(b). We observe high reflectivity values ($R>0.25$) for the reference whereas the reflectivity of the optimized structure does not exceed 0.05 over a wide range of incident angles (up to 80°). Such a result is of prime importance for a focusing device which requires isotropy not only for the effective negative index but also for the impedance matching between air and 2D PC. In order to check the efficiency of the designed antireflection grating, we simulate, with a 2D finite difference time domain (FDTD) method the electric field intensity distribution of the complete optimized structure. The result is shown in Fig. 1(d) and unambiguously shows that the negative refraction focusing regime is achievable with the design and a bright image spot is clearly visible. Note that when compared with simulations of the reference lens, the brightness of the image spot is clearly enhanced while its full width at half maximum along the transverse direction is preserved.

Then, we fabricated the optimized lens by using the nanoelectronics techniques on III-V semiconductors: heterostructure growth is made by molecular beam epitaxy, and e-beam lithography followed by inductively coupled plasma deep etching technique is used for nanopatterning the structures. More details about fabrication can be found elsewhere.[21] It is important here to note that fabricating the antireflection gratings with the accurate parameters *wb*, *hb*, and *ht* given by the design is a tricky task. For that reason we fabricated four optimized lenses with different values for *wb* and *ht* parameters, slightly varying from the ideal case. Due to technological limitations, *hb* parameter of the four samples is lower limited to $0.06a$ (28 nm). A scanning electron microphotograph (SEM) view of one of the typical fabricated structure is presented in Fig. 1(c). All the values of the fabricated and measured *wb* and *ht* parameters are mentioned hereafter in Fig. 2.

The optimized lenses have been characterized by a SNOM operating in collection mode.[22] The waveguide light injection is realized with a TE polarized tunable laser source (Anritsu TUNICS+CL/WB), and a near-field probe is scanned over the surface using piezoelectric stages with a shear-force feedback. The near-field probe consists in a pulled silica optical fiber with a 20 nm apex which locally detects the electric field intensity surrounding the nanostructure. Figure 2 shows the SNOM pictures of the four structures with different triangular pattern parameters and for an input wavelength of 1530 nm. We note that for the measurement representation, we used an illuminated view (and not a density plot with a colorscale) since the detected light intensity can differ from several orders of magnitude from one part of the picture to another one. The height scan of SNOM

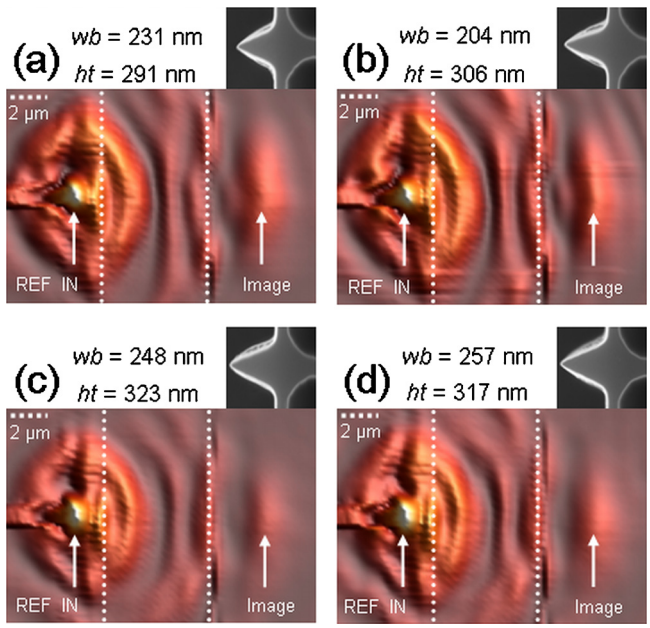

FIG. 2. (Color online) Unprocessed data SNOM pictures of the four optimized lenses at $\lambda=1530$ nm, plotted in illuminated view. Superimposed dotted lines reveal lenses interfaces position. For each picture, corresponding triangular pattern parameters and SEM view (plotted at the same scale as each other) are associated: (a) $wb=0.49a$, $hb=0.06a$, and $ht=0.61a$; (b) $wb=0.43a$, $hb=0.06a$, and $ht=0.64a$; (c) $wb=0.52a$, $hb=0.06a$, and $ht=0.68a$; (d) $wb=0.54a$, $hb=0.06a$, and $ht=0.67a$.

pictures is set to 4 nm above the waveguide and the 2D PC lens and to 1.5 μm above the substrate for all free space areas, which corresponds to the actual height of the InGaAsP guiding layer. One can observe in the pictures of Fig. 2, the negative refraction focusing regime of the four optimized lenses. Note that due to sample height and shear-force feedback scanning our near-field probe detects a source point (REF IN) slightly shifted from the very end of the waveguide. For each picture, we observe from left to right: REF IN, interference fringes related to wave propagation inside the nanostructure, and image point at 11 μm away from the end of the waveguide, which is the expected distance for the $n=-1$ regime. In order to estimate influence of our interface engineering, we measure on SNOM pictures the LTE for the four optimized lenses. Here, this figure of merit is defined as the ratio between image point and REF IN light intensity peak. Each peak value is averaged with the eight adjoining pixels of the corresponding SNOM picture. The four samples come from the same wafer with only one fabrication process and experimental conditions for SNOM characterization are also rigorously duplicated for all pictures of Fig. 2. Thus we can directly compare the various LTE we obtain: 21% [Fig. 2(b)], 18% [Fig. 2(a)], 14% [Fig. 2(d)], and 10% [Fig. 2(c)]. These values have also to be compared to the reference lens for which a LTE of 5% have been measured at the very best. This clearly evidences the influence of the interface engineering reported here with a four times enhancement of the LTE for the case of Fig. 2(b). The other results illustrate the extreme sensitivity of the optimal design to ensure impedance matching between air and 2D PC over a wide range of incident angles.

At last, to assess the wavelength sensitivity of the reported structure, we analyzed the spectral dependence of the LTE of the best optimized lens. We thus realize local near-field spectroscopy experiments[23] for the image point and the REF IN positions. We stop the near-field probe scan at these positions (height scan is set to 1.5 μm above the substrate) and record the intensity of the detected light as a function of the injected wavelength for the image point and for REF IN. The bare spectra are plotted in Figs. 3(b) and 3(c), and we present in Fig. 3(d) the normalized transmittance of the lens,

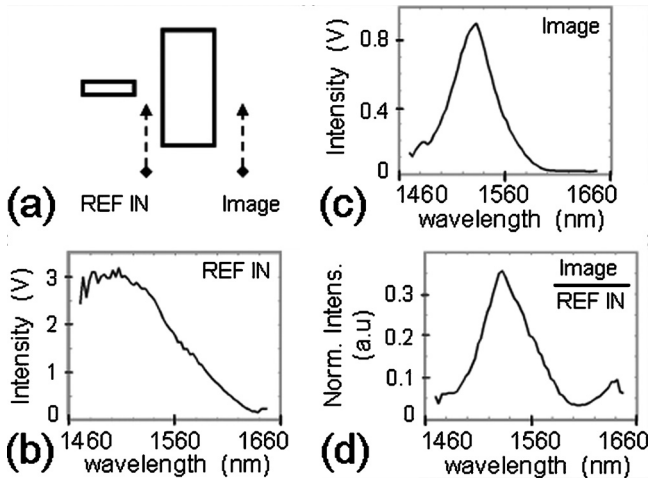

FIG. 3. Local near-field spectroscopy (1470 nm$<\lambda<$1650 nm) of the optimized lens ($wb=0.43a$, $hb=0.06a$, and $ht=0.64a$) with the higher LTE: (a) schematic top view, (b) spectral response for the REF IN position, (c) spectral response for the image point, and (d) normalized spectral response (maximal value at $\lambda=1533$ nm).

i.e., the ratio between image point and REF IN spectra. On the REF IN spectrum, a flat transmittance until the beginning of the detector cut-off at 1.55 μm (H10330 Hamamatsu NIR PMT Module) is measured whereas a Gaussian shape spectrum is recorded at the image point. As a consequence, this leads to a normalized spectrum with an optimal peak transmittance at $\lambda=1533$ nm in good agreement with the near-field observations. Finally, we note that the near-field spectroscopy experiment leads to a value of transmittance (35%) higher than the LTE measured on the pictures (21%). This mainly comes from the uncertainties of the near-field probe lateral position in the REF IN region for the spectroscopy experiment that could lead to an over evaluation of the LTE.

To summarize, we have presented PC flat lenses with interfaces engineered to improve their transmittance thanks to a broad angles impedance matching. The engineered interfaces consist in antireflection gratings designed to reduce the propagative waves reflectivity over a wide range of incident angles. The fabricated structures were measured in optical near-field and a four times enhancement of the LTE is reported. The results reported improve significantly the performances of PC flat lenses in terms of light transmission efficiency which is a key figure of merit for future applications in the field of free space focusing devices for optical interconnected nanosystems.

This work was partly supported by the project FANI funded by the Agence Nationale de la Recherche (ANR). G.S. would like to thank the Regional Council of Burgundy for financial support.

[1] V. G. Veselago, Sov. Phys. Usp. **10**, 509 (1968).
[2] J. B. Pendry, Phys. Rev. Lett. **85**, 3966 (2000).
[3] X. Zhang and Z. Liu, Nature Mater. **7**, 435 (2008).
[4] N. M. Litchinitser and V. M. Shalaev, J. Opt. Soc. Am. B **26**, B161 (2009).
[5] M. Notomi, Phys. Rev. B **62**, 10696 (2000).
[6] V. Veselago, L. Braginsky, V. Shklover, and C. Hafner, J. Comput. Theor. Nanosci. **3**, 189 (2006).
[7] J. Valentine, J. Li, T. Zentgraf, G. Bartal, and X. Zhang, Nature Mater. **8**, 568 (2009).
[8] A. Berrier, M. Mulot, M. Swillo, M. Qiu, L. Thylén, A. Talneau, and S. Anand, Phys. Rev. Lett. **93**, 073902 (2004).
[9] R. Chatterjee, N. C. Panoiu, K. Liu, Z. Dios, M. B. Yu, M. T. Doan, L. J. Kaufman, R. M. Osgood, and C. W. Wong, Phys. Rev. Lett. **100**, 187401 (2008).
[10] N. Fabre, L. Lalouat, B. Cluzel, X. Mélique, D. Lippens, F. de Fornel, and O. Vanbésien, Phys. Rev. Lett. **101**, 073901 (2008).
[11] C. Luo, S. G. Johnson, and J. D. Joannopoulos, Phys. Rev. B **68**, 045115 (2003).
[12] A. Martínez and J. Marti, Phys. Rev. B **71**, 235115 (2005).
[13] R. Moussa, Th. Koschny, and C. M. Soukoulis, Phys. Rev. B **74**, 115111 (2006).
[14] W. Śmigaj and B. Gralak, Phys. Rev. B **77**, 235445 (2008).
[15] W. Śmigaj, B. Gralak, R. Pierre, and G. Tayeb, Opt. Lett. **34**, 3532 (2009).
[16] B. D. F. Casse, W. T. Lu, R. K. Banyal, Y. J. Huang, S. Selvarasah, M. R. Dokmeci, C. H. Perry, and S. Sridhar, Opt. Lett. **34**, 1994 (2009).
[17] T. Matsumoto, K.-S. Eom, and T. Baba, Opt. Lett. **31**, 2786 (2006).
[18] L. Gan, Y.-Z. Liu, J.-Y. Li, Z.-B. Zhang, D.-Z. Zhang, and Z.-Y. Li, Opt. Express **17**, 9962 (2009).
[19] T. Decoopman, G. Tayeb, S. Enoch, D. Maystre, and B. Gralak, Phys. Rev. Lett. **97**, 073905 (2006).
[20] C. Croënne, N. Fabre, D. P. Gaillot, O. Vanbésien, and D. Lippens, Phys. Rev. B **77**, 125333 (2008).
[21] N. Fabre, S. Fasquel, C. Legrand, X. Mélique, M. Muller, M. François, O. Vanbésien, and D. Lippens, Opto-Electron. Rev. **14**, 225 (2006).
[22] D. Gérard, L. Berguiga, F. de Fornel, L. Salomon, C. Seassal, X. Letartre, P. Rojo-Romeo, and P. Viktorovitch, Opt. Lett. **27**, 173 (2002).
[23] B. Cluzel, E. Picard, T. Charvolin, E. Hadji, L. Lalouät, F. de Fornel, C. Sauvan, and P. Lalanne, Appl. Phys. Lett. **88**, 051112 (2006).